BAYERO JOURNAL OF ENGINEERING AND TECHNOLOGY (BJET) VOL.16 No.2, MAY, 2021
PP 37-47 ISSN: 2449 – 0539

FATIGUE ANALYSIS IN MODULAR MULTILEVEL CONVERTER USING RAINFLOW ALGORITHM

Nasiru B. Kadandani

Department of Electrical Engineering, Bayero University, PMB 3011, Kano, Nigeria
Email: nbkadandani.ele@buk.edu.ng

ABSTRACT

Modular multilevel converter (MMC) is composed of several semiconductor switches and capacitors. However, these basic components of MMC are fragile especially when operated in harsh environment. As such, the resulting fatigue of the converter need to be estimated so that the converter can be replaced before complete failure. One of the parameters that determines the lifetime of the converter is the junction temperature of the semiconductor switches which varies during operation and generates temperature swings. In this paper, an electro-thermal model for estimating the junction temperature of MMC is developed and rainflow algorithm is used to identify the fatigue parameters from the temperature profile; namely temperature swings, mean value of the temperature and the number of temperature cycles. Using these parameters, the number of cycles to failure were computed based on Coffin-Manson-Arrhenius lifetime model. The entire system including the control strategy was simulated in MATLAB® using Simulink® and PLECS® toolboxes. The results show that temperature swing is the main critical stressor of the converter, as such, can be used to plan maintenance or replacement before complete failure occurs. The temperature estimation was validated on a laboratory prototype MMC using type-K thermocouples and KEYSIGHT LXI Agilent 34972A BenchLink Data Logger.

Keywords: Modular multilevel converter (MMC); semiconductor switch; junction temperature; rainflow algorithm; sub-module (SM).

1. INTRODUCTION

Modular Multilevel Converter (MMC) being a power electronic converter (PEC) is designed with semiconductor switches and capacitors which have very high failure rate as per the survey conducted in (Yang et al., 2011) where it was established that the main stress comes from environment, transients, and heavy loads, which need to be taken into consideration during the design stage and normal operation.

Insulated gate bipolar transistor (IGBT) power module is an exemplary semiconductor used in MMC. It consists of many layers of different materials with different coefficients of thermal expansion (CTE). Figure 1 shows the basic structure of a typical wire-bonded IGBT power module. As can be seen in the figure, on top of the baseplate is direct-copper bonded (DCB) ceramic substrate, while the silicon chip is soldered on the DCB.

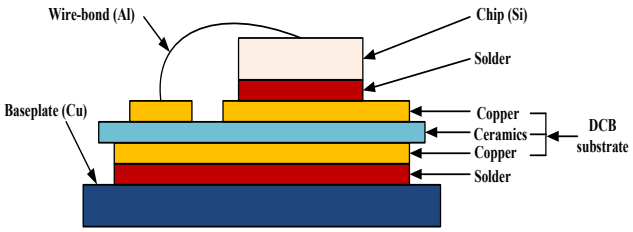

Figure 1: Structure of IGBT Power Module (Volke & Hornkamp, 2011)

The difference in the CTE within the DCB results in temperature variation which translates into mechanical stress within the IGBT module (Choi & Blaabjerg, 2018). The thermal

cycling resulting from the temperature variation results in repeated heating and cooling making disparately joined materials to expand and shrink at different rates. This expansion and shrinking leads to failure. The substrate layers attached to the baseplate can be subjected to solder fatigue due to thermal cycling. The most vulnerable points are wire bonds and silicon interconnections, DCB substrate and baseplate solder joint, and silicon and DCB substrate solder joint. Figure 2 gives a summary of the failure mechanism of IGBT.

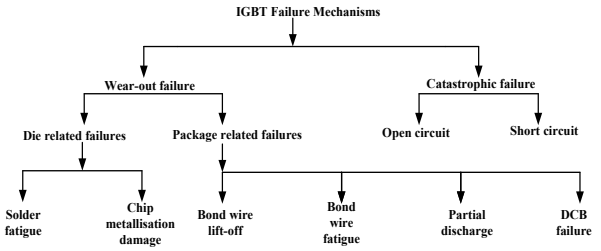

Figure 2: Failure Classification in IGBT

The wear-out failure is as a result of long term degradation and normally arise due to uneven thermal impedance in the power semiconductor devices (Vernica, Choi, Wang, & Blaabjerg, 2020). Bond-wire lift-off have been identified as the major failure mechanism under this category (Ciappa & Fichtner, 2000). For example, during thermal cycling, the disparately joined materials expands and shrinks due to cooling and heating. As a result of this, a *wire-bond lift-off failure* will be induced to the device. In the event of degradation however, the thermal resistance of the module increases thereby increasing the temperature of the module. This rise in temperature accelerates the wire-bond lift-off failure (Scheuermann & Schmidt, 2011). For high voltage IGBTs however, *partial discharge* have been identified as the common wear-out failure (Mitic & Lefranc, 2002). This type of failure typically occur on IGBT manufactured with imperfect etching of silicon and it manifest itself on the metallization edges in the silicon gel (Fabian, Hartmann, & Hamidi, 2005). *Bond-wire fatigue* on the other hand is as a result of temperature swing stress coming from power dissipation in the silicon die due to CTE mismatch which is translated into fatigue across the wire pad and the wire bonding (Choi & Blaabjerg, 2018).

The catastrophic failures however occur as a result of single overstress event due to excessive current flowing through the device (Ahsan, Hon, Batunlu, & Albarbar, 2020). They are unpredictable and difficult to handle, as such, they result in huge damage to the device within a very short period of time. Catastrophic failures are of two forms; open-circuit and short-circuit (Wu, Blaabjerg, Wang, Liserre, & Iannuzzo, 2013). The result of an experiment conducted in (Lefebvre, Khatir, & Saint-Eve, 2005) shows that repetitive short circuit events do not destroy IGBT immediately, rather it reduces the operational life of the device. However, at higher short circuit energy close to the critical value, the IGBT fail at the first short circuit test. In similar development, the research conducted in (Palmer, Rajamani, & Joyce, 2000) shows that single high short circuit events results in complete failure of the IGBT.

To improve the reliability of semiconductors, modified packaging technology was proposed in (Haumann, Rudzki, Osterwald, Becker, & Eisele, 2013; Scheuermann & Beckedahl, 2008) where the aluminum bonding wire was replaced by copper bonding wire. In this way, the CTE mismatch was reduced. In a similar development, (M. Wang & al) proposed molybdenum buffers as means of improving the reliability of IGBT modules.

Capacitors are other fragile components of MMC. Failure sources in capacitors can be from the operating conditions (such as temperature, voltage and current) or from other factors (such as mechanical stress, material wear out and design defect) (H. Wang & Blaabjerg, 2014). As with semiconductors, the failure can be classified as wear out or catastrophic depending on the causes and nature of the failure. In the case of electrolytic capacitors, failure can be induced due to vibration, shock or thermal expansion causing disconnection of the capacitor terminals from the system . Ceramic capacitors are even less reliable due to their brittleness nature to the extent that failure can be induced by mechanical stress during thermal cycling (Andersson, Kristensen, Miller, Gloor, & Iannuzzo, 2018).

Several attempts have been made to reduce the failure rate of DC link capacitors and improve their reliability. An approach

based on ripple current minimization control was proposed in (Freitas, Jacobina, & Santos, 2010) while a hybrid solution was proposed in (Brubaker, Hage, Hosking, Kirbie, & E. D. Sawyer, 2013), where two capacitors of different frequencies are combined to provide DC link for a 250kW inverter. Another approach was proposed in (Krein, Balog, & Mirjafari, 2012; H. Wang, Chung, & Liu, 2014; R. Wang et al., 2011) where a ripple power port was added in order to reduce the total energy requirement of the DC link capacitor. On the contrary, researchers in (Chen, Afridi, & Perreault, 2013), considered replacing the DC link capacitor with an energy buffer and were able to achieve energy buffering ration of over 90%.

The junction temperature of the semiconductor devices in MMC system is the leading factor that determines the lifetime of the converter. When the converter is in operation, the junction temperature of the switches are subjected to variation based on the loading current. The resulting temperature swings can induce failure by stressing the wire bonding and die attach solder (Y. Huang, Luo, Xiao, & Liu, 2019; Yongle, Yifei, Fei, Binli, & Xin, 2020). In devices with regular loading, temperature cycles can be easily counted leading to quick estimation of the lifetime of the system. However, such cycles (successive maxima and minima) cannot be easily counted in systems with irregular loading history such as IGBT junction temperature. Thus, the fatigue analysis of devices with irregular loading profiles requires proper algorithms for cycle counting. Example of such algorithms include simple range counting, peak counting, level-crossing counting, and rainflow counting (Musallam & Johnson, 2012). The loading profile of MMC is variable and unpredictable, hence, their reliability design requires an efficient cycle counting method to identify all the equivalent full and half cycles within the irregular load profile. Once all the cycles are identified, the lifetime of the converter can be estimated by conventional cycle-based lifetime model. A three point rainflow counting algorithm is employed here for cycle counting in such irregular loading history which has the advantage of having very small relative error and can provide average value (Perpina, Jorda, Vellvehi, Rebollo, & M. Mermet-Guyennet, 2011).

The remaining part of this paper is organized as follows. Section 2 presents methodology in terms of MMC and its control method, the method of estimating junction temperature of the semiconductor switches and fatigue analysis. Section 3 presents results and discussion. Section 4 concluded the article.

2. METHODOLOGY

2.1. MMC and its Control Method

A circuit schematic of three phase MMC is shown in fig. 3. Each phase leg is made up of two non-coupled buffer inductors and two stacks of multiple bidirectional cascaded-cells known as submodules (SMs).

A centralized method of capacitor voltage balancing is employed in regulating the submodule capacitor voltages to their reference values. As can be seen in figure 4, the method takes into account the capacitor voltages and arm current polarities to select certain SMs for certain switching states. The modulation involves measuring and sorting SM capacitor voltages within an arm for every pulse width modulation (PWM) period. In this process, the SMs with lowest capacitor voltages are activated when the arm current is positive. This will enable the SM capacitors to be charged and increase their voltages. Conversely, the SMs with highest capacitor voltages are activated when the arm current is negative, in this case, the SM capacitors are discharged and their voltages decreased.

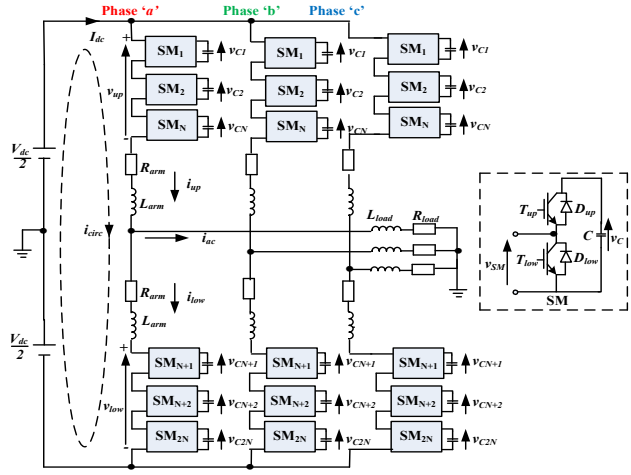

Figure 3: Circuit Configuration of Three Phase MMC

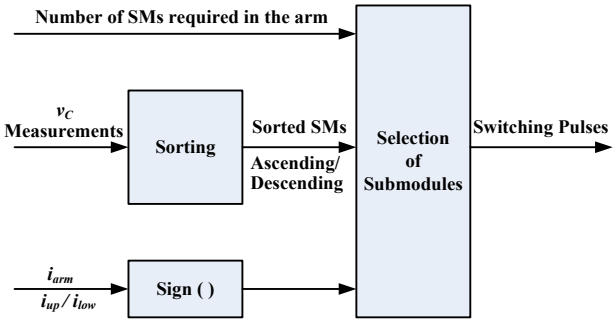

Figure 4: Block Diagram of Sorting Algorithm for Capacitor Voltage Balancing Control

2.2. Junction Temperature Estimation

The junction temperature can be estimated based on the mission profile. This is achieved by feeding the later into an electro-thermal model block implemented in PLECS toolbox within MATLAB. The semiconductor switch used is FF75R12RT4 from Infineon (Infineon, 2013). The electro-thermal model comprises of power loss and thermal model blocks as detailed in figure 5.

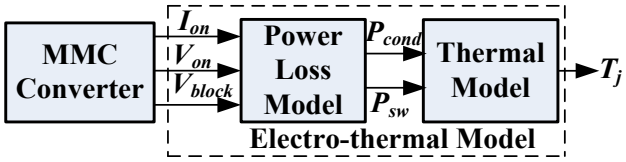

Figure 5: Flow Chart for Junction Temperature Estimation

An electro-thermal model was developed to estimate the junction temperature of the semiconductor devices. In the simulation, this was implemented using piece-wise linear electric circuit simulator (PLECS®) toolbox within MATLAB®. In the experimental set-up however, type-K thermocouples were used to measure the temperature.

The thermal model block is based on Foster model. The choice is based on the availability of the thermal coefficients of the parallel RC elements that were provided in the manufacturer's datasheet. The model is derived from the transient thermal impedance information in the datasheet. The thermal impedance of the semiconductor switch can be expressed in the following form:

$$Z_{th}(t) = \sum R_i(1 - e^{\frac{-t}{\tau_i}}) \quad (1)$$

where R_i is the equivalent thermal resistance and τ_i is the thermal time constant for each conduction path.

Considering the four conduction paths of the semiconductor switch, (1) can be written in Laplace form as follows:

$$Z_{th}(t) = \frac{R_{th1}}{\tau_1 s + 1} + \frac{R_{th2}}{\tau_2 s + 1} + \frac{R_{th3}}{\tau_3 s + 1} + \frac{R_{th4}}{\tau_4 s + 1} \quad (2)$$

The thermal capacitance can be expressed in terms of the thermal resistance and thermal time constants as:

$$C_{thi} = \frac{\tau_1}{R_{thi}} \quad (3)$$

A schematic of the thermal model used in this study is shown in figure 6.

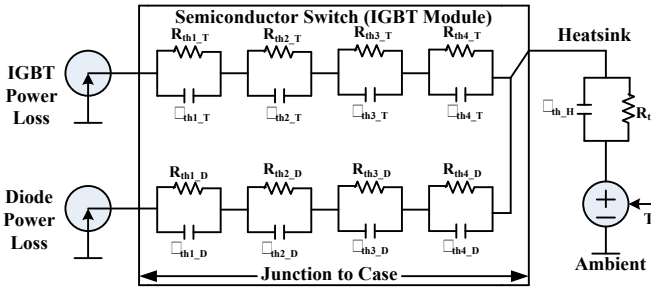

Figure 6: Thermal Model of IGBT Semiconductor Module

2.3. Fatigue Analysis

Figure 7 shows the block diagram for analyzing the fatigue of MMC. *Rainflow cycle counting algorithm* was applied on the turning points of the junction temperature profile and three thermal parameters were evaluated; amplitude of the temperature swing, the mean value of the maximum junction temperature and the range of the temperature swing. *Fatigue analysis* was carried out based on Coffin-Manson-Arrhenius analytical lifetime model which gives the number of cycles to failure based on temperature swing and average value of the temperature. *The number of cycles to failures were t*hen quantified using Coffin-Manson-Arrhenius lifetime model.

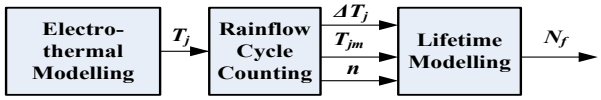

Figure 7: Flow Chart for Fatigue Analysis in MMC

2.4. Temperature Cycle Counting Using Rainflow Algorithm

Rainflow algorithm was introduced in 1968 by Matuishi and Endo (Matsuishi & Endo, 1968) while trying to count the cycles and half cycles of strain-time signals. The analogy of the algorithm was derived from the rain falling on a pagoda and running down the edges of a roof. As can be seen in figure 8, the load stress represents a series of roofs on which the water falls as the time axis is vertical. The peak and valley of the stress are assumed to be the source of water dropping down the pagoda and are located on the left and right sides respectively. The algorithm is based on the stress-strain behavior of the material. The load reversals are combined in such a way that a cycle is defined as closed hysteresis loop and each loop has mean stress and strain range for comparison with constant amplitude. The physical basis of this algorithm is therefore the closed loop hysteresis in the temperature profile (H. Huang & Mawby, 2013). Apart from the method proposed by Matuishi and Endo, there are also other rainflow counting techniques such as three and four-point counting technique - all of which ended up with the same result. In this research, the three point counting technique is used because it is computationally fast.

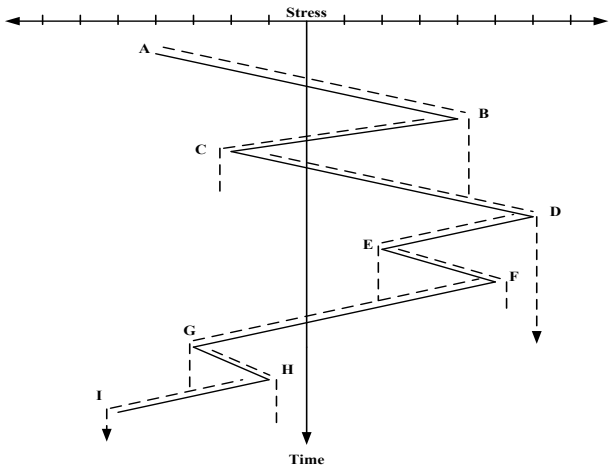

Figure 8: Rainflow on a Load Sequence

In this research, a three-point rainflow counting technique is used. The algorithm repeatedly checks three consecutive peaks/valley (say A, B and C) of a loading history to determine if a cycle is formed or not. First, the loading history (i.e the junction temperature profile) has to be rearranged to contain only the maxima and minima and begins with the one with highest absolute magnitude; be it the highest peak or the lowest valley. A cycle check is then conducted on every three consecutive points. When a cycle is counted, points A and B are discarded from the loading history and the remaining points are connected together. The cycle check is then repeated until all the points are exhausted.

Two rules are used for cycle identification using the three-point technique as illustrated for hanging and standing cycles shown in figure 9 (Lee, Barkey, & Kang, 2011).

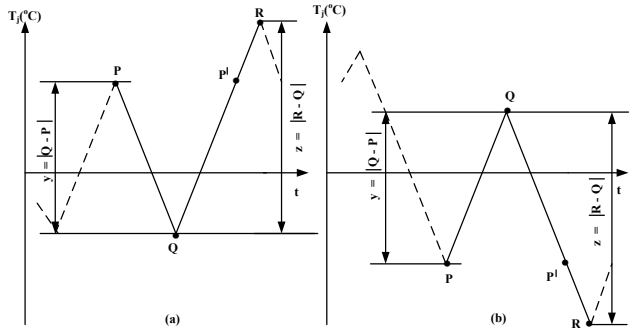

Figure 9: Three Point Rainflow Counting Technique (a) hanging Cycle, (b) Standing Cycle

- A cycle is counted if the loading history doesn't starts from A and x ≥ y, in which case, A and B are discarded.
- A half cycle or reversal is counted from A to B if the loading history starts from A and x ≥ y, in which case, only A discarded.

When the cycle identification is completed, rainflow algorithm provides three parameters that are stored in a matrix. The parameters are; cycle amplitudes, T_{ja}, ranges or mean value of the cycles, T_{jm}, and the number of the identified cycles.

For an identified cycle shown in figure 10 with T_{jmax} as maxima and T_{jmin} as minima, then the following definitions hold:

The amplitude of the cycle, T_{ja} is:

$$T_{ja} = \left|\frac{T_{jmax} - T_{jmin}}{2}\right| \quad (4)$$

The mean value of the cycle, T_{jm} is:

$$T_{jm} = \frac{T_{jmax} + T_{jmin}}{2} \quad (5)$$

The range of the identified cycle is:

$$\Delta T_j = \left|T_{jmax} - T_{jmin}\right| \quad (6)$$

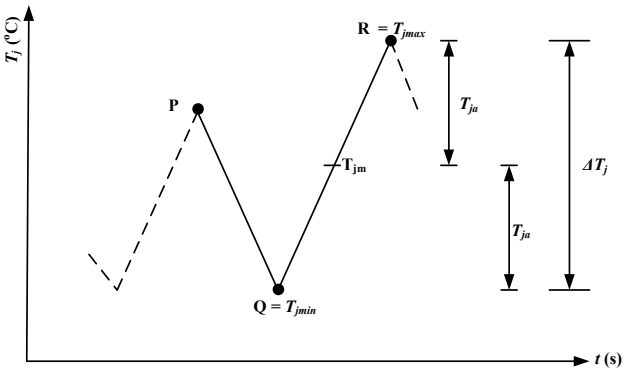

Fig. 10: One Cycle of Irregular Temperature Loading Showing Rainflow Parameters

2.5. Fatigue Modelling Using Coffin Manson Arrhenius Lifetime Model

The relationship between the lifetime (in number of cycles), the mean temperature and the amplitude of the temperature was proposed in (Held, Jacob, Nicoletti, Scacco, & Poech, 1997). The equation, often referred to as Coffin-Manson-Arrhenius lifetime model is given by:

$$N_f(T_{jm}, \Delta T_{jm}) = A * \Delta T_j^{\alpha} * \exp\left(\frac{E_a}{k_B * T_{jm}}\right) \quad (7)$$

where N_f is the expected number of cycle before failure, T_{jm} is the mean (average) value of the temperature, ΔT_{jm} is the amplitude (temperature range), E_a is the activation energy = $9.89*10^{-20}$ (J), k_B is Boltzman constant = $1.38066*10^{-23}$ (J/K), while A and α are constants and are module dependent.

3. RESULTS AND DISCUSSION

The converter control combined with electro-thermal model were implemented in MATLAB® using Simulink® and PLECS® toolboxes based on system parameters of table 1.

Table 1: Parameters of the MMC Prototype

Parameter	Value
Converter Rating	1MVA
Number of Submodule Per Arm	20
Submodule Capacitance	10mF
Capacitor Voltage Reference	1kVA
Input DC Link Voltage	20kV
Output AC Voltage Reference	10kV
Carrier Frequency	2kHz
Modulation Index	0.9

3.1. Estimated Junction Temperature

Even though the computed power loss is unidirectional, but it is equivalent to current in electrical domain. Upon feeding the power losses into the thermal block, the junction temperatures of the semiconductor switches were estimated. Figure 11 shows the junction temperature of the SMs.

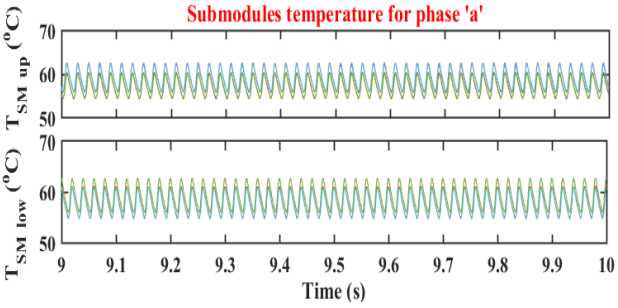

(a)

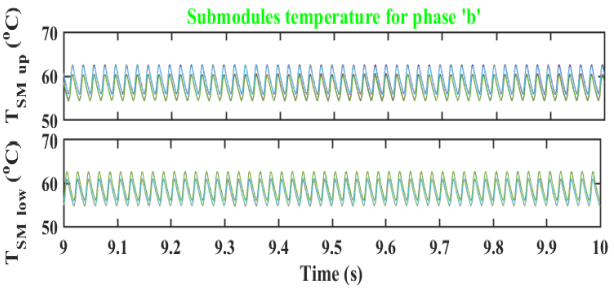

(b)

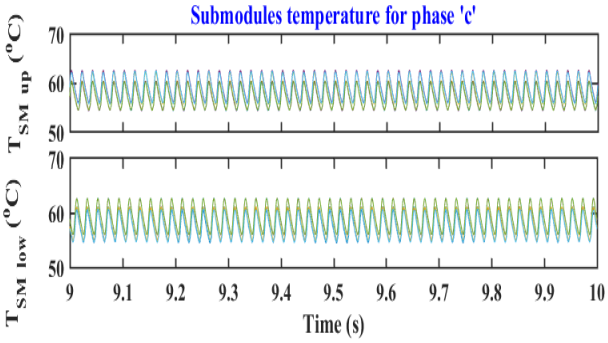

(c)

Figure 11: Measured Junction Temperature of Submodules (a) Phase A, (b) Phase B and (c) Phase C

3.2. Results from Rainflow Algorithm

Figure 12 shows the junction temperature profile of one SM based on the mission profile. The lower IGBT in each sub-module has the highest junction temperature. This is expected as it is the most stressed component of any sub-module.

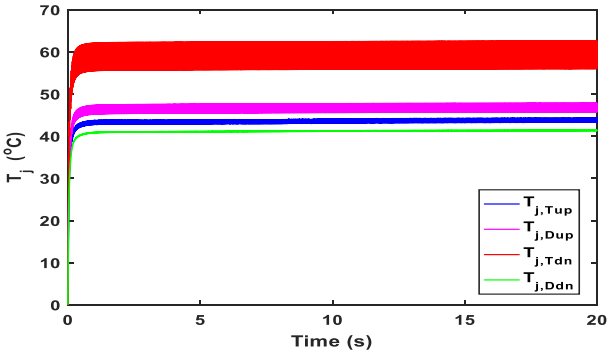

Fig 12: Junction Temperature of One SM

The local extrema of its junction temperature profile were first identified. Rainflow algorithm was then applied to the turning points and the algorithm identified all the temperature cycles, their amplitude, mean value and range. The results are shown in figure 13 through 15. Fig. 13 is a rainflow matrix that depicts the distribution of temperature and average temperature among the identified cycles. Figure 14 and 15 present the rainflow histogram that show the distribution of temperature range among the identified cycles and the

corresponding damages respectively. The number of cycles to failure was computed using eqn (7) as $6.61x10^{15}$. This means the converter can withstand $6.61x10^{15}$ cycles under the given load conditions before it fails completely. This figure can be used to plan maintenance.

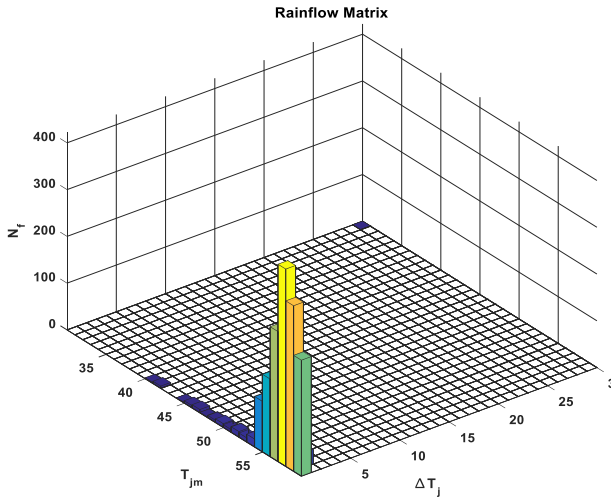

Fig. 13: Rainflow 3D Matrix

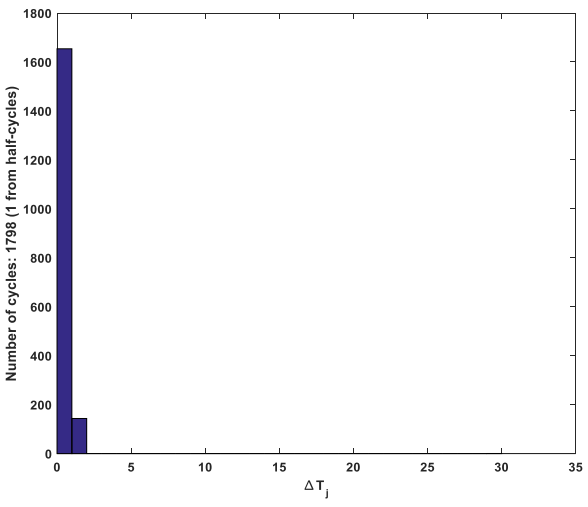

Fig. 14: Rainflow Histogram of Distribution of Temperature Range among Identified Cycles

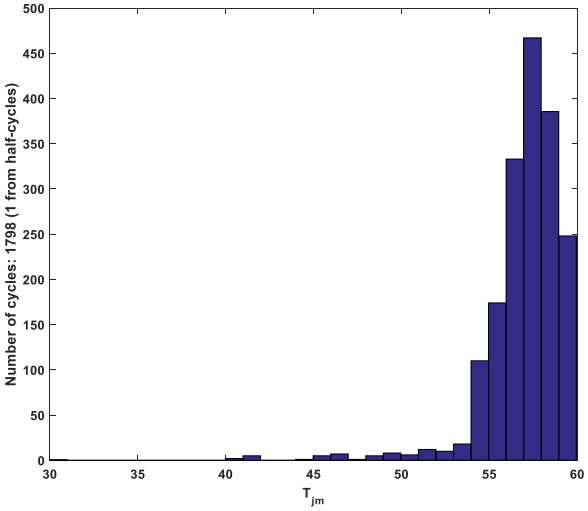

Fig. 15: Rainflow Histogram of damage caused by Temperature Range among Identified Cycles

3.3. Experimental Validation

As shown in figure 16, the laboratory prototype is a single phase MMC with four submodules per arm.

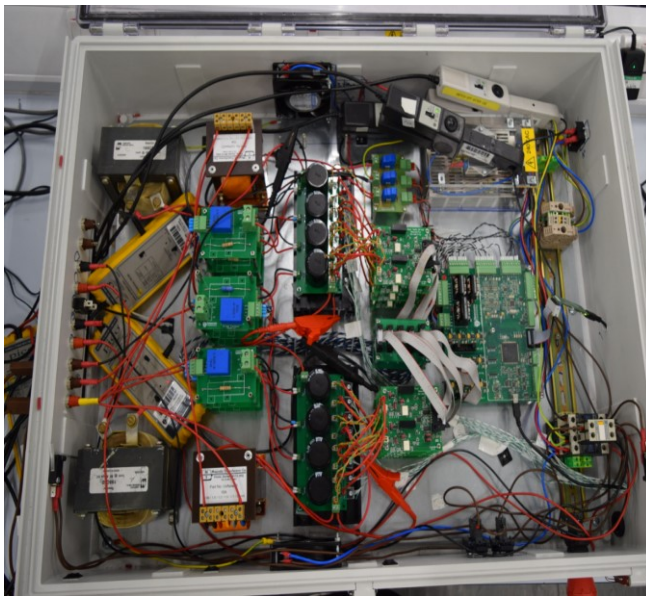

Figure 16: Experimental Set-up

The control algorithm was implemented in code composer studio ("Code Composer Studio,") using TMS320F28377D

microcontroller board (Datasheet) and MATLAB GUI. The IGBT used is GT20J341 from Toshiba (TOSHIBA, 2012). The case temperature of the IGBT switches were measured using Type-K thermocouples interphase with KEYSIGHT LXI Agilent 34972A BenchLink Data Logger / Switch Unit (Datasheet). Figure 17 shows the connection and communication structure for temperature measurement while figure 18 shows the measured junction temperature of the converter SMs.

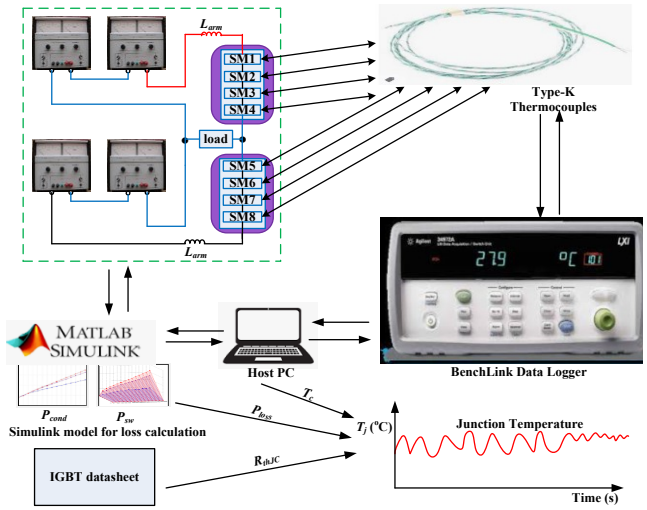

Figure 17: Connection and Communication Structure for Temperature Measurement

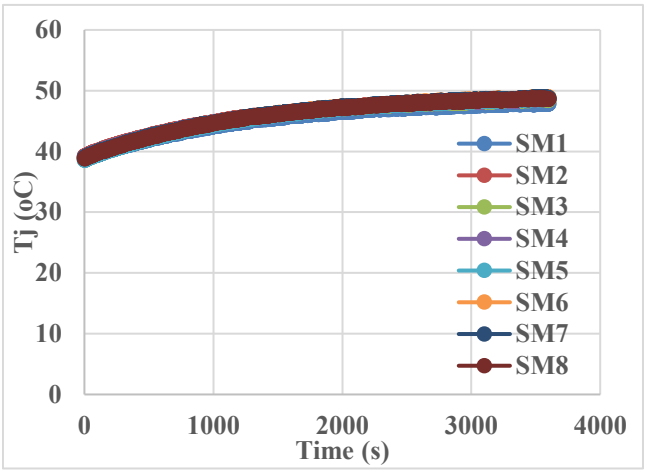

Figure 18: Temperature of Submodules

4. CONCLUSION

The paper has investigated a physics-based approach of estimating the number of cycles to failure in MMC. The lifetime model used in the research has taken temperature swing (which is the root causes of the failure of the semiconductor switches) into consideration, as such, the method is said to be highly reliable. An electro-thermal model block developed in PLECS was used to estimate the junction temperature of the semiconductor switches and rainflow algorithm in conjunction with Coffin-Manson- Arrhenius law were applied to the turning points of the junction temperature profiles for cycle counting and computing the number of cycles to failure.

REFERENCES

Ahsan, M., Hon, S. T., Batunlu, C., & Albarbar, A. (2020). Reliability Assessment of IGBT Through Modelling and Experimental Testing. *IEEE Access, Vol. 8*, pp. 39561-39573.

Andersson, C., Kristensen, O., Miller, S., Gloor, T., & Iannuzzo, F. (2018). Lock-in Thermography Failure Detection on Multilayer Ceramic Capacitors After Flex Cracking and Temperature–Humidity–Bias Stress. *IEEE Journal of Emerging and Selected Topics in Power Electronics, Vol. 6, No. 4*, pp. 2254-2261.

Brubaker, M. A., Hage, D. E., Hosking, T. A., Kirbie, H. C., & E. D. Sawyer. (2013). Increasing the Life of Electrolytic Capacitor Banks Using Integrated High Performance Film Capacitors. *Europe Power Conversion Intelligent Motion (PCIM) Nuremberg, Germany*.

Chen, M., Afridi, K. K., & Perreault, D. J. (2013). Stacked Switched Capacitor Energy Buffer Architecture. *IEEE Transactions on Power Electronics, Vol. 28, No. 11*, pp. 5183–5195.

Choi, U., & Blaabjerg, F. (2018). Separation of Wear-out Failure Modes of IGBT Modules in Grid-Connected Inverter Systems. *IEEE Transactions on Power Electronics, Vol. 33, No. 7*, pp. 6217-6223.

Ciappa, M., & Fichtner, W. (2000). Lifetime Prediction of IGBT Modules for Traction Applications. *IEEE 38th Annual International Reliability Physics Symposium*, pp. 210-216.

Code Composer Studio. *https://software-dl.ti.com/ccs/esd/documents/ccs_downloads.html*.

Datasheet. 34972A LXI Data Acquisition / Data Logger Switch Unit. *https://literature.cdn.keysight.com/litweb/pdf/34972-90010.pdf*.

Datasheet. DSP-TI TMS320F28377D. *http://www.ti.com/lit/ds/symlink/tms320f28377d-ep.pdf*.

Fabian, J., Hartmann, S., & Hamidi, A. (2005). Analysis of Insulation Failure Modes in High Power IGBT Modules. *2005 Fourtieth IAS Annual Meeting Industry Applications Conference*, pp. 799-805.

Freitas, I. S., Jacobina, C. B., & Santos, E. C. d. (2010). Single-phase to Single-Phase Full-Bridge Converter Operating With Reduced AC Power in the DC-Link Capacitor. *IEEE Transaction on Power Electronics, Vol. 5, No. 2*, pp. 272–279.

Haumann, S., Rudzki, J., Osterwald, F., Becker, M., & Eisele, R. (2013). Novel Bonding and Joining Technology For Power Electronics - Enabler For Improved Lifetime, Reliability, Cost And Power Density. *2013 Twenty-Eighth Annual IEEE Applied Power Electronics Conference and Exposition (APEC), Long Beach, CA*, pp. 622-626.

Held, M., Jacob, P., Nicoletti, G., Scacco, P., & Poech, M.-. (1997). Fast Power Cycling Test of IGBT Modules in Traction Application. *The Second International Conference on Power Electronics and Drive Systems, Singapore, Vol. 1*, pp. 425-430

Huang, H., & Mawby, P. A. (2013). A Lifetime Estimation Technique for Voltage Source Inverters. *IEEE Transactions on Power Electronics, Vol. 28*, No. 8, pp. 4113-4119.

Huang, Y., Luo, Y., Xiao, F., & Liu, B. (2019). Failure Mechanism of Die-Attach Solder Joints in IGBT Modules Under Pulse High-Current Power Cycling. *IEEE Journal of Emerging and Selected Topics in Power Electronics, Vol. 7, No. 1*, pp. 99-107.

Infineon. (2013). IGBT Module FF75R12RT4 Data Sheet.

Krein, P., Balog, R., & Mirjafari, M. (2012). Minimum Energy and Capacitance Requirements for Single-Phase Inverters and Rectifiers Using a Ripple Port. *IEEE Transactions on Power Electronics, Vol. 27, No. 11*, pp. 4690–4698.

Lee, Y. L., Barkey, M. E., & Kang, H. T. (2011). Metal Fatigue Analysis Handbook. *Elsevier Inc*.

Lefebvre, S., Khatir, Z., & Saint-Eve, F. (2005). Experimental Behaviour of Single-Chip IGBT and COOLMOS Devices Under Repetitive Short-Circuit Conditions. *IEEE Transactions on Electron Devices*, pp. 276-283.

Matsuishi, M., & Endo, T. (1968). Fatigue of Metals Subjected to Varying Stress. *Proceeding of Japan Society of Mechanical Engineers, Fukuoka, Japan*, 3pp. 7–40.

Mitic, G., & Lefranc, G. (2002). Localisation of Electrical-Insulation and Partial-Discharge Failures of IGBT Modules. *IEEE Transactions on Industry Applications*, pp. 1453-1458.

Musallam, M., & Johnson, C. M. (2012). An Efficient Implementation of the Rainflow Counting Algorithm for Life Consumption Estimation. *IEEE Transactions on Reliability, Vol. 61*, No. 4, pp. 978-986.

Palmer, P., Rajamani, H., & Joyce, J. (2000). Behaviour of IGBT Modules Under Short Circuit Conditions. *2000 IEEE Industry Applications Conference*, pp. 3010-3015.

Perpina, X., Jorda, X., Vellvehi, M., Rebollo, J., & M. Mermet-Guyennet. (2011). Long-term Reliability of Railway Power Inverters Cooled by Heat-Pipe Based Systems. *IEEE Transactions on Industrial Electronics, Vol. 58, No. 7*, pp. 2662–2672.

Scheuermann, U., & Beckedahl, P. (2008). The Road to the Next Generation Power Module - 100% Solder Free Design. *5th International Conference on Integrated Power Electronics Systems, Nuremberg, Germany,* pp.1-10.

Scheuermann, U., & Schmidt, R. (2011). Impact of Solder Fatigue on Module Lifetime in Power Cycling Tests. *Proceedings of the 2011 14th European Conference on Power Electronics and Applications, Birmingham*, pp. 1-10.

TOSHIBA. (2012). IGBT GT20J341 Datashet.

Vernica, I., Choi, U. M., Wang, H., & Blaabjerg, F. (2020). Wear-out Failure of an IGBT Module in Motor Drives due to Uneven Thermal Impedance of Power Semiconductor Devices. *Microelectronics Reliability, 114*.

Volke, A., & Hornkamp, M. (2011). IGBT Modules. *Infineon Technologies AG, Munich, Germany*.

Wang, H., & Blaabjerg, F. (2014). Reliability of Capacitors for DC-Link Applictions in Power Electronic Converters - An Overview. *IEEE Transactions on Industry Applications, Vol. 50, No. 5*, pp. 3569-3578.

Wang, H., Chung, H. S. H., & Liu, W. (2014). Use of a Series Voltage Compensator for Reduction of the DC-link Capacitance in a Capacitor-Supported System. *IEEE Transactions on Power Electronics, Vol. 29, No. 3*, pp. 1163–1175.

Wang, M., & al, e. Reliability Improvement of a Double-Sided IGBT Module by Lowering Stress Gradient Using Molybdenum Buffers. *IEEE Journal of Emerging and Selected Topics in Power Electronics, Vol. 7, No. 3*, pp. 1637-1648.

Wang, R., Wang, F., Boroyevich, D., Burgos, R., Lai, R., Ning, P., & Pajashekara, K. (2011). A High Power Density Single-Phase PWM Rectifier With Active Ripple Energy Storage. *IEEE Transactions on Power Electronics, Vol. 26, No. 5*, pp. 1430-1443.

Wu, R., Blaabjerg, F., Wang, H., Liserre, M., & Iannuzzo, F. (2013). Catastrophic Failure and Fault-Tolerant Design of IGBT Power Electronic Converters - An Overview. *IECON 2013 - 39th Annual Conference of the IEEE Industrial Electronics Society, Vienna*, pp. 507-513.

Yang, S., Bryant, A., Mawby, P., Xiang, D., Ran, L., & Tavner, P. (2011). An Industry-Based Survey of Reliability in Power Electronic Converters. *IEEE Transactions on Industry Applications, Vol. 47*, No. 3, pp. 1441-1451.

Yongle, H., Yifei, L., Fei, X., Binli, L., & Xin, T. (2020). Physics of Failure of Die-attach Joints in IGBTs Under Accelerated Aging: Evolution of Micro-Defects in Lead-Free Solder Alloys. *Microelectronics Reliability, 109*.